

A microscopic Ginzburg–Landau theory and singlet ordering in Sr₂RuO₄

Glenn Wagner,^{1,2} Henrik S. Røising,^{1,3,*} Felix Flicker,^{1,4,5} and Steven H. Simon¹

¹*Rudolf Peierls Center for Theoretical Physics, Oxford OX1 3PU, United Kingdom*

²*Kavli Institute for Theoretical Physics, University of California Santa Barbara, CA 93106, USA*

³*Nordita, KTH Royal Institute of Technology and Stockholm University,
Roslagstullbacken 23, SE-106 91 Stockholm, Sweden*

⁴*School of Physics and Astronomy, Cardiff University, Cardiff CF24 3AA, United Kingdom*

⁵*School of Mathematics, University of Bristol, Bristol BS8 1TW, United Kingdom*

(Dated: June 6, 2022)

The long-standing quest to determine the superconducting order of Sr₂RuO₄ (SRO) has received renewed attention after recent nuclear magnetic resonance (NMR) Knight shift experiments have cast doubt on the possibility of spin-triplet pairing in the superconducting state. As a putative solution, encompassing a body of experiments conducted over the years, a $d + ig$ -wave order parameter caused by an accidental near-degeneracy has been suggested [S. A. Kivelson et al., npj Quantum Materials **5**, 43 (2020)]. Here we develop a general Ginzburg–Landau theory for multiband superconductors. We apply the theory to SRO and predict the relative size of the order parameter components. The heat capacity jump expected at the onset of the second order parameter component is found to be above the current threshold deduced by the experimental absence of a second jump. Our results tightly restrict theories of $d + ig$ order, and other candidates caused by a near-degeneracy, in SRO. We discuss possible solutions to the problem.

I. INTRODUCTION

26 years ago the layered perovskite Sr₂RuO₄ (SRO) was found to harbour unconventional superconductivity below the modest critical temperature $T_c \approx 1.5$ K¹. Its superconducting order has been widely believed to be chiral p -wave². This belief was primarily rooted in the absence of a drop in the nuclear magnetic resonance (NMR) Knight shift³, and the indications of time-reversal symmetry-breaking (TRSB) found in muon spin relaxation⁴ (μ SR) and Kerr rotation⁵ experiments. Chiral p -wave superconductors open the possibility of hosting Majorana zero modes which have intriguing applications to topological quantum computation⁶.

Over the years, the number of experimental results not conforming with the chiral p -wave hypothesis have accumulated⁷. Among observations difficult to explain within the chiral p -wave paradigm are indications of gap nodes inferred from heat capacity^{8,9}, heat conductivity¹⁰ and scanning tunneling microscopy measurements (STM)¹¹, and the absence of a T_c -cusp under uniaxial strain^{12,13}. A peak in the accumulated evidence was reached when the NMR Knight shift experiment was repeated^{14,15}, now finding a substantial reduction in the spin susceptibility at low temperature. This has launched a renewed focus on the compound, both experimentally^{16–21} and theoretically^{22–32}.

The new NMR experiments^{14,15} appear reconcilable with a number of even-parity (pseudo-)spin singlet order parameters and possibly the helical p -wave (pseudo-)spin triplet order parameters. However, the options are being narrowed down as thermodynamic shear elastic measurements¹⁹ and μ SR¹⁸ suggest that the superconducting order is likely two-component, at least at temperatures well below T_c . A very recent NMR experiment at low magnetic fields casts further doubt on any odd-parity or

der parameter²⁰, leaving spin-singlet pairing as the most likely scenario. Recently, two putative solutions to the long-standing puzzles have been proposed.

A chiral d -wave order parameter (irreducible representation (irrep) E_g of D_{4h} in the group theory nomenclature) could explain TRSB and the observed jump in the shear elastic modulus c_{66} ¹⁹. It was shown that a chiral d -wave can be stabilized by including certain k_z -dependent spin-orbit coupling (SOC) terms at sufficiently large Hund's coupling²⁶. However, the prevailing belief has been that the material is effectively two-dimensional (2D)^{7,33}, a belief which has recently been examined and to some extent confirmed^{22,24,34}. Furthermore, the horizontal line node that the $d_{xz} + id_{yz}$ order possesses, would likely conflict with the experimental evidence of vertical line nodes^{10,11}.

Another possibility, solving the latter issue, is an accidental (near-)degeneracy between a $d_{x^2-y^2}$ and $g_{xy(x^2-y^2)}$ -wave order parameter²⁸. This scenario has the potential of explaining both features of the temperature vs. strain phase diagram, indications of TRSB, vertical line nodes, and the shear elastic modulus jump. However, although various theories find d -wave order as the leading instability^{22–24,27,30}, an exotic g -wave order becoming competitive currently lacks support from calculations using the relevant band structure. Moreover, an accidental near-degeneracy would imply the presence of a secondary, possibly small, heat capacity jump at a temperature $T_{\text{TRSB}} < T_c$. Despite intensive search for a second jump in high-precision measurements¹⁶, such an observation remains elusive (*cf.* the successful observation in the case of UPt₃³⁵).

Here we address the feasibility of a $d + ig$ order parameter in SRO by taking on a microscopic perspective to discuss the heat capacity anomaly. We first develop the framework for a general multiband, multi-component

Ginzburg–Landau (GL) theory where the expansion coefficients depend on the band structure. Our theory reduces to that of Gor’kov³⁶ in the one-band low-filling limit. Using band and gap structures applicable to SRO we find, by numerical minimization of the free energy, that the d - and g -wave components prefer to be of comparable magnitude at low temperature. We calculate the expected secondary heat capacity jump and evaluate it numerically as a function of the order parameter component sizes. The results predict a second jump much larger than what is seen experimentally, meaning a large degree of fine-tuning would be required in any possible $d + ig$ scenario. The same conclusion is reached for other near-degeneracy options.

Finally, variations of the general theory developed here could also prove to have applications to exotic (chiral) superconductors³⁷ outside the scope of SRO, like FeAs-based systems³⁸, UTe₂^{39,40}, and URu₂Si₂^{41,42}.

II. THEORY: MULTIBAND GINZBURG–LANDAU

In this section we develop a generic expansion of the free energy in the order parameter close to the critical temperature for a multiband superconductor. We initiate the approach for a single-component order parameter in Sec. II A and vindicate it in the low-filling limit in Sec. II B. In Sec. II C we extend the theory to the case of two nearly degenerate single-component (pseudo-)spin singlet order parameters consistent with the symmetries

of a tetragonal lattice.

A. Single-component theory

To set the stage for the derivation, we shall consider spin-singlet Cooper pairing terms H_{SC} as perturbations to the normal-state Hamiltonian H_{N} close to the critical temperature, where

$$H_{\text{N}} = \sum_{\mu, \sigma, \mathbf{p}} \xi_{\mu}(\mathbf{p}) c_{\mu\sigma}^{\dagger}(\mathbf{p}) c_{\mu\sigma}(\mathbf{p}), \quad (1)$$

$$H_{\text{SC}} = \sum_{\mu, \sigma, \mathbf{p}} \sum'_{\mathbf{q}} [\Delta_{\mu}(\mathbf{q}) c_{\mu\sigma}^{\dagger}(\mathbf{p} + \frac{\mathbf{q}}{2}) c_{\mu\bar{\sigma}}^{\dagger}(-\mathbf{p} + \frac{\mathbf{q}}{2}) + \text{h.c.}]. \quad (2)$$

Above, $\xi_{\mu}(\mathbf{k})$ is the dispersion of band μ ($\mu = \alpha, \beta, \gamma$ in the case of SRO), and $\sigma = \uparrow, \downarrow$ denotes (pseudo-)spin, with $\bar{\sigma}$ denoting the opposite spin. The sum over \mathbf{p} runs over the first Brillouin zone, whereas the sum over \mathbf{q} runs over the Fermi surface sheet $|\xi_{\mu}(\mathbf{q})| < \omega_c \sim k_B T$, where $\omega_c \ll W$ is an electronic cutoff small compared to the bandwidth W , as indicated with a prime on the sum. Lastly, $\Delta_{\mu}(\mathbf{q})$ is the (pseudo)spin-singlet order parameter of band μ at momentum \mathbf{q} . Considering only intra-band terms is justified if the superconducting gap is small compared to the energy separation of the bands at the Fermi level, which indeed is satisfied in SRO where these energy scales are on the order of 0.5 meV¹¹ and 100 meV³⁴, respectively.

Proceeding with the Ginzburg–Landau (GL) approach we expand the free energy density in the (single-component) order parameter close to the critical temperature³⁶ (see also Refs. 27, 38, 43–46):

$$F_1[\{\Delta_{\mu}(\mathbf{r})\}] = \sum_{\mu} \left(\frac{1}{V^2} \int_{\mathbf{r}, \mathbf{r}'} \Delta_{\mu}(\mathbf{r})^* \alpha_{\mu}(\mathbf{r} - \mathbf{r}', T) \Delta_{\mu}(\mathbf{r}') \right. \\ \left. + \frac{1}{V^4} \int_{\mathbf{r}_1, \dots, \mathbf{r}_4} \Delta_{\mu}(\mathbf{r}_1)^* \Delta_{\mu}(\mathbf{r}_2)^* \beta_{\mu}(\mathbf{r}_4 - \mathbf{r}_1, \mathbf{r}_4 - \mathbf{r}_2, \mathbf{r}_4 - \mathbf{r}_3, T) \Delta_{\mu}(\mathbf{r}_3) \Delta_{\mu}(\mathbf{r}_4) \right) \quad (3)$$

$$= \sum_{\mu} \left(\sum'_{\mathbf{q}} \alpha_{\mu}(\mathbf{q}, T) |\Delta_{\mu}(\mathbf{q})|^2 + \sum'_{\mathbf{q}_1, \mathbf{q}_2, \mathbf{q}_3} \beta_{\mu}(\mathbf{q}_1, \mathbf{q}_2, \mathbf{q}_3, T) \Delta_{\mu}^*(\mathbf{q}_1) \Delta_{\mu}^*(\mathbf{q}_2) \Delta_{\mu}(\mathbf{q}_3) \Delta_{\mu}(\mathbf{q}_1 + \mathbf{q}_2 - \mathbf{q}_3) \right),$$

where we used the Fourier expansion $\Delta_{\mu}(\mathbf{r}) = \sum'_{\mathbf{q}} \Delta_{\mu}(\mathbf{q}) e^{i\mathbf{r} \cdot \mathbf{q}}$, and where V is the total volume (area) in 3D (2D). As the superconducting phase is entered, the corrections to the normal state free energy, $\Delta F = F_{\text{SC}} - F_{\text{N}}$, are caused by the superconducting terms of Eq. (2). The corrections can be evaluated and equated with Eq. (3) using the Gibbs average of the S -

matrix^{36,47,48},

$$\Delta F = -T \ln \langle S \rangle, \quad (4)$$

$$S = \mathcal{T}_{\tau} \exp \left(- \int_0^{\beta} d\tau H_{\text{SC}}(\tau) \right), \quad (5)$$

where $\beta = 1/T$ (with $k_B = 1$), $\tau = -i\beta$ is imaginary time, and \mathcal{T}_{τ} is the time-ordering operator. The loop expansion of ΔF , involving only connected diagrams, is

given by

$$\begin{aligned} \Delta F &= -T(\langle S \rangle_c - 1) \\ &\approx \frac{T}{2!} \int_0^\beta d\tau_1 \int_0^\beta d\tau_2 \langle \mathcal{T}_\tau [H_{\text{SC}}(\tau_1) H_{\text{SC}}(\tau_2)] \rangle_c \\ &\quad + \frac{T}{4!} \int_0^\beta d\tau_1 \cdots \int_0^\beta d\tau_4 \langle \mathcal{T}_\tau [H_{\text{SC}}(\tau_1) \cdots H_{\text{SC}}(\tau_4)] \rangle_c. \end{aligned} \quad (6)$$

Pictorially this consists of closed connected diagrams with only external Δ legs produced by combinations of the Feynman diagram of Fig 1.

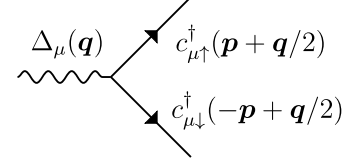


FIG. 1. The (pseudo)spin-singlet Cooper pair operator shown diagrammatically as a two-fermion composite operator.

To calculate the first and second terms of Eq. (6) for a weakly coupled superconductor (which is valid near the critical temperature), bare Green's functions are introduced as⁴⁵

$$G_\mu(\mathbf{p}, \tau_1 - \tau_2) = -\langle \mathcal{T}_\tau c_{\mu\uparrow}(\mathbf{p}, \tau_1) c_{\mu\uparrow}^\dagger(\mathbf{p}, \tau_2) \rangle. \quad (7)$$

This can be expressed in the Matsubara representation: $G_\mu(\mathbf{p}, \omega_n) = 1/(i\omega_n - \xi_\mu(\mathbf{p}))$, with fermionic Matsubara frequencies $\omega_n = \frac{\pi}{\beta}(2n+1)$ for integer n . The second and fourth order contributions of Eq. (6), with corresponding diagrams shown in Fig. 2 (a) and (b), are given upon evaluation by

$$\begin{aligned} \Delta F^{(2)} &= -T \sum_\mu \sum_{\mathbf{q}}' |\Delta_\mu(\mathbf{q})|^2 \sum_{\mathbf{p}, n} G_\mu\left(\mathbf{p} + \frac{\mathbf{q}}{2}, \omega_n\right) G_\mu\left(-\mathbf{p} + \frac{\mathbf{q}}{2}, -\omega_n\right) \\ &\quad + T_c \sum_\mu \sum_{\mathbf{q}}' |\Delta_\mu(\mathbf{q})|^2 \sum_{\mathbf{p}, n} G_\mu\left(\mathbf{p} + \frac{\mathbf{q}}{2}, \omega_n\right) G_\mu\left(-\mathbf{p} + \frac{\mathbf{q}}{2}, -\omega_n\right) \Big|_{T=T_c}, \end{aligned} \quad (8)$$

$$\begin{aligned} \Delta F^{(4)} &= \frac{T_c}{2} \sum_\mu \sum_{\mathbf{q}_1, \mathbf{q}_2, \mathbf{q}_3}' \Delta_\mu^*(\mathbf{q}_1) \Delta_\mu^*(\mathbf{q}_2) \Delta_\mu(\mathbf{q}_3) \Delta_\mu(\mathbf{q}_1 + \mathbf{q}_2 - \mathbf{q}_3) \\ &\quad \times \sum_{\mathbf{p}, n} G_\mu(-\mathbf{p}, -\omega_n) G_\mu(\mathbf{p} + \mathbf{q}_1, +\omega_n) G_\mu(-\mathbf{p} + \mathbf{q}_3 - \mathbf{q}_1, -\omega_n) G_\mu(\mathbf{p} + \mathbf{q}_1 + \mathbf{q}_2 - \mathbf{q}_3, \omega_n) \Big|_{T=T_c}, \end{aligned} \quad (9)$$

respectively. In $\Delta F^{(2)}$ we subtracted off the contribution evaluated at T_c to ensure that ΔF has a well-defined minimum for $T < T_c$. The fourth order term, shown in Fig. 2 (b), is evaluated at T_c . The expressions in Eq. (8) and (9) show that the GL coefficients α_μ and β_μ on the first line of Eq. (3) are generally relative position dependent, albeit translationally invariant, in real space. The expressions for the full momentum-dependent GL coefficients in reciprocal space are listed in Appendix A.

B. Evaluation in the low-filling limit

The expressions of Eq. (8) and (9) can be well approximated in the low-filling limit. At low filling and temperature the phase space is restricted and the following two approximations are reasonable: (i) neglect the \mathbf{q} -dependence of the Green's functions (assuming spatially uniform GL coefficients), and (ii) assume that the mo-

mentum sums of Eq. (9) are dominated by the contributions with $\mathbf{q}_1 = \mathbf{q}_2 = \mathbf{q}_3$. The frequency sums of Eq. (8) and (9) are evaluated analytically, and we arrive at the following expressions for the GL coefficients by comparing with Eq. (3):

$$\alpha_\mu(T, T_c) = -V \int \frac{d\mathbf{p}}{(2\pi)^d} \left(\frac{\tanh[\xi_\mu(\mathbf{p})/(2T)]}{2\xi_\mu(\mathbf{p})} - \frac{\tanh[\xi_\mu(\mathbf{p})/(2T_c)]}{2\xi_\mu(\mathbf{p})} \right) \quad (10)$$

$$\beta_\mu(T_c) = \frac{V}{2T_c^3} \int \frac{d\mathbf{p}}{(2\pi)^d} h(\xi_\mu(\mathbf{p})/T_c), \quad (11)$$

upon replacing the momentum sums by $\sum_{\mathbf{p}} \rightarrow V \int \frac{d\mathbf{p}}{(2\pi)^d}$, where V is the unit cell volume. Above, we introduced the function

$$h(x) \equiv \frac{\sinh x - x}{4x^3(1 + \cosh x)}. \quad (12)$$

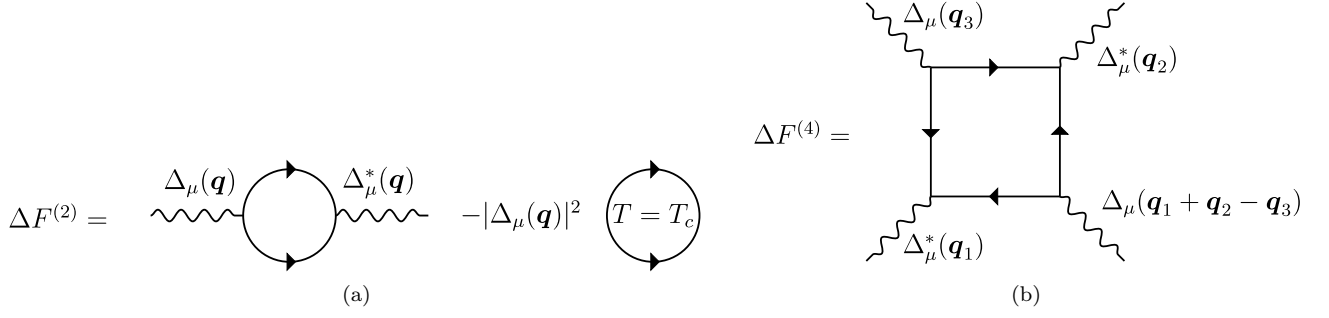


FIG. 2. The (a) second order and (b) fourth order diagrams contributing to the free energy of Eq. (6). The algebraic expressions corresponding to (a) and (b) are given in Eq. (8) and (9), respectively.

Next, we evaluate Eq. (10) and (11) for quadratic bands in 2D, $\xi_\mu(\mathbf{p}) = \frac{p^2}{2m_\mu}$, with $p = |\mathbf{p}|$ and m_μ being the effective mass of band μ . In the low-filling limit, the Brillouin zone integrals can be replaced by $\int d\mathbf{p} \rightarrow \int_0^\infty dp p \int_0^{2\pi} d\phi$. For the coefficients α_μ we assume that $T/T_c - 1 \ll 1$ and retain the leading term in a Taylor expansion. The result is (see Appendix B for details)

$$\alpha_\mu = \frac{\rho_\mu}{2} \left(\frac{T}{T_c} - 1 \right), \quad (13)$$

$$\beta_\mu = \frac{\rho_\mu}{T_c^2} \frac{7\zeta(3)}{32\pi^2}, \quad (14)$$

with $\rho_\mu = Vm_\mu/(2\pi)$ being the density of states and ζ the Riemann zeta function. This is equivalent to the result of Gor'kov³⁶.

Repeating the above exercise for linearly dispersing bands, $\xi_\mu(\mathbf{p}) = v_\mu p$, results instead in

$$\alpha_\mu = \rho_\mu \ln 2 \left(\frac{T}{T_c} - 1 \right), \quad (15)$$

$$\beta_\mu = \frac{\rho_\mu}{16T_c^2}, \quad (16)$$

where $\rho_\mu = VT_c/(2\pi v_\mu^2)$.

C. Two-component theory

As an extension of the theory of Eq. (3) we next consider two order parameters $\Delta_{a\mu}$ and $\Delta_{b\mu}$ with critical temperatures T_c and $T'_c < T_c$, respectively. The indices a and b are symmetry indices, referring to distinct irreps of the applicable point group. We shall focus on the tetragonal point group D_{4h} , for which the relevant one-dimensional irreps are listed in Table I and visualised in Fig. 3.

As a further specification we shall consider a and b to be one-dimensional pseudo-spin singlet irreps. In this case, the free energy to quartic order takes the following

TABLE I. One-dimensional, even-parity (pseudo-spin singlet) irreducible representations of the tetragonal point group D_{4h} ⁴⁹. Lattice harmonics of order parameters are listed in the Balian–Werthamer basis⁵⁰, $\Delta_{\sigma\sigma'} = [id_0(\theta)\sigma_y]_{\sigma\sigma'}$, where θ is the polar angle (2D)⁵¹.

Irrep	Name	Lattice harmonics of $d_0(\theta)$
A_{1g}	s'	$\sum_{n=1}^{\infty} a_n \cos(4n\theta)$
A_{2g}	$g_{xy(x^2-y^2)}$	$\sum_{n=0}^{\infty} b_n \sin([4n+4]\theta)$
B_{1g}	$d_{x^2-y^2}$	$\sum_{n=0}^{\infty} c_n \cos([4n+2]\theta)$
B_{2g}	d_{xy}	$\sum_{n=0}^{\infty} d_n \sin([4n+2]\theta)$

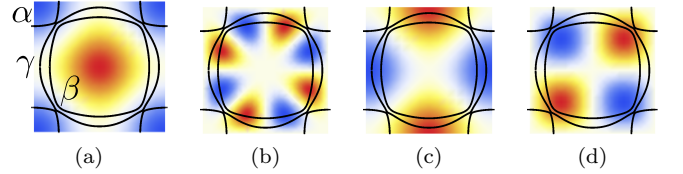


FIG. 3. Symmetries of the even-parity order parameters in channel (a) A_{1g} , (b) A_{2g} , (c) B_{1g} , (d) B_{2g} . The black lines display the Fermi surface applicable to the three-band case of Sr_2RuO_4 , where the three bands are denoted by α , β , and γ . The Fermi surface is obtained using tight-binding parameters listed in Appendix C, as extracted from density functional theory^{13,52}.

form in reciprocal space:

$$F_2[\{\Delta_{a\mu}, \Delta_{b\mu}\}] = \sum_{\mu} \left(\sum_{\mathbf{q}} \alpha'_{\mu}(\mathbf{q}, T, T_c) |\Delta_{a\mu}(\mathbf{q})|^2 + \alpha_{\mu}(\mathbf{q}, T, T'_c) |\Delta_{b\mu}(\mathbf{q})|^2 + \sum_{\mathbf{q}_1, \mathbf{q}_2, \mathbf{q}_3} \beta'_{\mu}(\mathbf{q}_1, \mathbf{q}_2, \mathbf{q}_3, T_c) \sum_{ijkl} f_{ijkl} \Delta_{i\mu}^*(\mathbf{q}_1) \Delta_{j\mu}^*(\mathbf{q}_2) \times \Delta_{k\mu}(\mathbf{q}_3) \Delta_{l\mu}(\mathbf{q}_1 + \mathbf{q}_2 - \mathbf{q}_3) \right), \quad (17)$$

where $f_{aaaa} = f_{aabb} = f_{bbaa} = f_{abab} = f_{abba} = f_{baab} = f_{baba} = f_{bbbb} = 1$ and all other $f_{ijkl} = 0$ such that the

individual terms all respect the D_{4h} symmetries. Diagrammatically, the order parameters involved in Fig. 2 now acquire symmetry labels with the external legs corresponding to the various terms of Eq. (17).

III. APPLICATION TO SRO

In this section we apply the theory developed in Sec. II to the multiband case of SRO. In Sec. III A we calculate the temperature-dependent order parameter weights. This is contrasted with the calculation of Sec. III B, where we estimate the heat capacity jump expected at the onset of a second order parameter component as a function of the two component sizes.

A. The relative order parameter weight

To minimize the free energy of Eq. (17), we employ the gap ansätze listed in Tab. I. Specifically, we fit the ansätze to the order parameters resulting from the microscopic weak-coupling calculation of Ref. 24, thereby including order parameter anisotropies expected for SRO (see Appendix D for details). For the band structure we work with a (2D) three-band model (which includes spin-orbit coupling), based on density functional theory^{13,52}. This model is presented in Appendix C. We feed in the band structure of the α , β , and γ bands and evaluate Eqs. (8) and (9) numerically using Monte-Carlo integration with the two-parameter theory $F_2[\{\Delta_0\Delta_{a\mu}(\mathbf{k}), i\Delta_0 X\Delta_{b\mu}(\mathbf{k})\}] \equiv F_2[\Delta_0, X]$. The function $F_2[\Delta_0, X]$ is minimized over the two scalar arguments: the overall gap size Δ_0 and the relative weight X as a function of temperature. In Eq. (17) the $d + ig$ hypothesis is addressed by specifying $a = B_{1g}$ and $b = A_{2g}$.

The resulting form of $X(T)$ determined from minimization of F_2 is shown in Fig. 4, employing a realistic three-band dispersion described in Appendix C, with the corresponding Fermi surface shown in Fig. 3. The value of X quickly tends to a value > 1 as the temperature is lowered through $T_{\text{TRSB}} < T'_c$. Notably, the momentum-independent approximation does not agree well with the exact theory which has momentum-dependent GL coefficients.

B. The heat capacity anomaly

In a recent μ SR experiment¹⁸ two temperature scales were probed under uniaxial strain: T_c and T_{TRSB} as determined from the heat capacity jump and the abrupt change in the muon spin relaxation rate, respectively. The results indicate that (i) there is a sharp onset of TRSB at $T_{\text{TRSB}} \lesssim T_c$ (with $T_{\text{TRSB}}/T_c \approx 0.94$ when averaged over four samples), and (ii) that the two temperatures split increasingly under uniaxial strain.

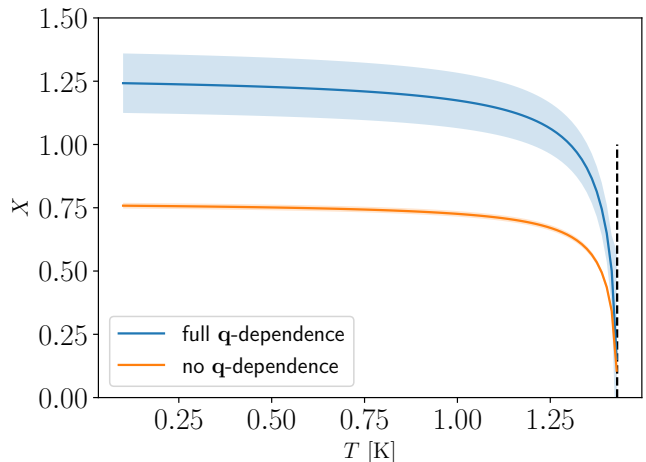


FIG. 4. The weight $X(T)$, with an order parameter of the form $\Delta(\mathbf{k}) = \Delta_0(T)[\Delta_{B_{1g}\mu}(\mathbf{k}) + iX(T)\Delta_{A_{2g}\mu}(\mathbf{k})]$ for $T_{\text{TRSB}} = 1.43$ K (indicated by the dashed line) and $T_c = 1.48$ K. The approximate result is obtained from the momentum-independent GL coefficients Eqs. (10) and (11), whereas the exact result is obtained from the full momentum-dependent expressions Eqs. (8) and (9). The standard deviation of the result over ten Monte-Carlo runs is indicated by the shaded region.

However, measurements of the heat capacity resolved under uniaxial strain did not observe any secondary heat capacity jump, as would be expected with the onset of a second order parameter component^{16,18,53}. This resulted in the experimental bound, deduced from the measurement resolution^{16,18}, that any secondary jump would have to be less than about 1/20 of the primary one⁵⁴.

In this section we incorporate the above constraints by assuming that $T_{\text{TRSB}} = 1.43$ K and $T_c = 1.48$ K, and we emphasize that the results below remain fairly insensitive to small variations in T_{TRSB} . The heat capacity is evaluated with

$$C(T) = 2 \sum_{\mu} \sum_{\mathbf{k}} E_{\mu}(\mathbf{k}) \frac{df[E_{\mu}(\mathbf{k})]}{dT}, \quad (18)$$

with quasiparticle energies $E_{\mu}(\mathbf{k}) = (\xi_{\mu}^2 + |\Delta_{\mu}(\mathbf{k})|^2)^{\frac{1}{2}}$ and $f(z) = (1 + \exp(\beta z))^{-1}$ denoting the Fermi function. Assuming that the order parameter takes the form

$$\Delta(\mathbf{k}) = \Delta_{0,a} (1 - T/T_c)^{\frac{1}{2}} \Delta_a(\mathbf{k}) + i\Delta_{0,b} (1 - T/T_{\text{TRSB}})^{\frac{1}{2}} \Delta_b(\mathbf{k}) \quad (19)$$

(where band indices are suppressed) leads to the following expressions for the ratio of the secondary ($T = T_{\text{TRSB}}$)

to the primary ($T = T_c$) heat capacity jump²⁸:

$$\eta = \frac{\Delta C}{T_{\text{TRSB}}}\Big|_{T=T_{\text{TRSB}}}/\frac{\Delta C}{T_c}\Big|_{T=T_c} = \left(\frac{\Delta_{0,b}}{\Delta_{0,a}}\frac{T_c}{T_{\text{TRSB}}}\right)^2 \frac{\langle |\Delta_b(\mathbf{k})|^2 I(\mathbf{k}) \rangle_{\text{FS}}}{\langle |\Delta_a(\mathbf{k})|^2 \rangle_{\text{FS}}}, \quad (20)$$

$$I(\mathbf{k}) = \int_0^\infty du \left(\cosh \left[(u^2 + z(\mathbf{k})^2)^{\frac{1}{2}} \right] \right)^{-2}, \quad (21)$$

$$z(\mathbf{k}) = \Delta_{0,a} \Delta_a(\mathbf{k}) (1 - T_{\text{TRSB}}/T_c)^{\frac{1}{2}} / (2T_{\text{TRSB}}). \quad (22)$$

A colour plot of η for the $d + ig$ scenario ($a = B_{1g}$ and $b = A_{2g}$) is shown in Fig. 5. For the order parameters we use those obtained in Ref. 24, as well described by the three leading lattice harmonics listed in Appendix D. In Fig. 5 (b) we display the expected specific heat anomaly for parameters close to the experimental threshold, and in Fig. 5 (c) we show the specific heat for the GL solution of Sec. III A. In both cases the second heat capacity jump is dominant on the β -band which is a result of the gap being dominant on that band, combined with the fact that the density of states on the β -band is about 31% of the total in our model (which is twice as much as for the α -band which has the next-largest gap).

The results suggest that the order parameter of Eq. (19) appears consistent with experiments^{16,19} when $\Delta_{0,A_{2g}} \lesssim 0.3\Delta_{0,B_{1g}}$. This should be contrasted with the results of minimizing the GL theory in Fig. 4, for which $\Delta_{0,A_{2g}} \gtrsim \Delta_{0,B_{1g}}$ and the second heat capacity jump is greater than the experimental threshold. The result indicates that, in order to be consistent with experiment, a second order parameter component would need to be smaller than that predicted with our theory. We note, however, that the second heat capacity jump only depends on the non-analyticity of $|\Delta|$ at $T = T_{\text{TRSB}}$, which can in principle result in jumps of either sign when resolved over bands for the GL solution (as seen in Fig. 5 (c)), see Appendix E. It is therefore conceivable that a band cancellation could explain a vanishingly small second jump.

An ultrasound spectroscopy experiment recently mapped out the symmetry-resolved elastic tensor of SRO¹⁹. The results indicate discontinuous jumps in the compressional elastic moduli (A_{1g}) and in only one of the shear elastic moduli (B_{2g}). This observation would be consistent with a two-component order parameter where the two components, if belonging to different irreps, form bilinears only in these two channels. As deduced from the direct product table of the irreps in Table I, this would be the case for $B_{1g} + iA_{2g}$ and for $A_{1g} + iB_{2g}$. However, only the first of these cases would have symmetry-protected line nodes and thereby offer an explanation of the observed heat capacity⁸, heat conductivity¹⁰, and STM measurements¹¹. In Appendix D we examine the order parameter combination $A_{1g} + iB_{2g}$ for completeness. The same conclusion that the heat capacity jump is inconsistent with the experimental data is reached for this order parameter, and the qualitative features remain fairly insensitive to the precise order parameters used.

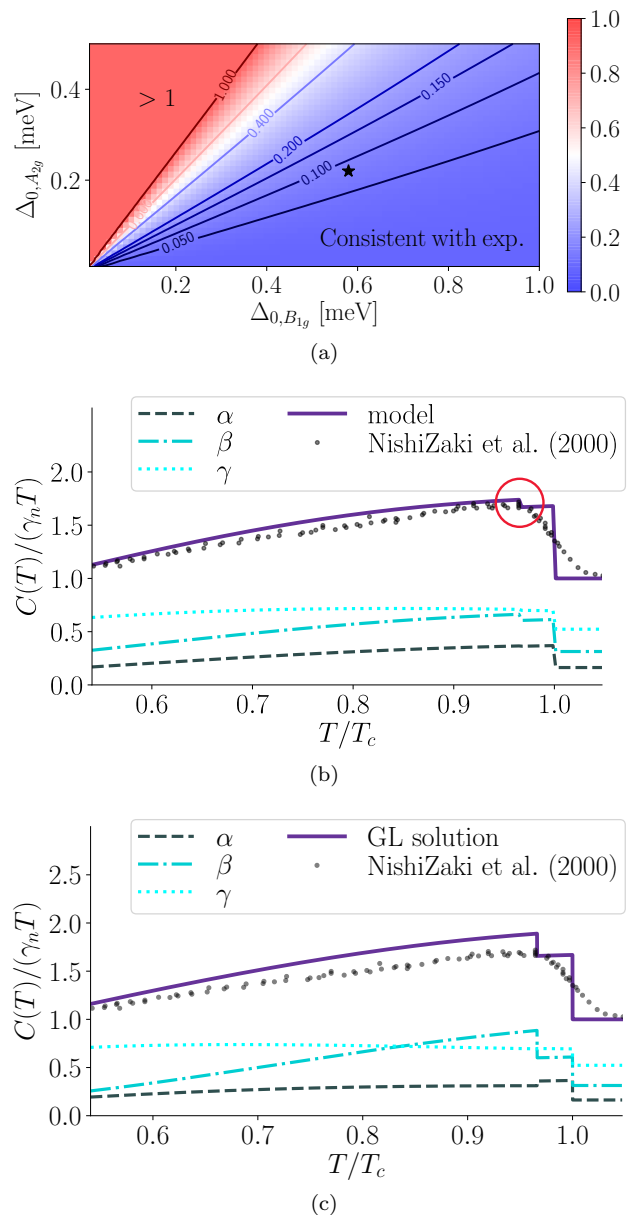


FIG. 5. Heat capacity anomaly for a $B_{1g} + iA_{2g}$ order parameter in SRO. Panel (a): Contour lines for the ratio of the second heat capacity jump to the primary heat capacity jump, η , from Eq. (20), with $T_{\text{TRSB}} = 1.43$ K and $T_c = 1.48$ K using order parameters with three lattice harmonics (see Appendix D). Experimental thresholds for η are currently at 0.05; a larger value should have already been detected^{16,19}. For the dispersion we use the (2D) three-band model listed in Appendix C. Panel (b): Specific heat at the point marked with “★” in panel (a). Panel (c): Specific heat for the GL solution of Sec. III A. The normalized specific heat per temperature is compared to the data of Ref. 8. The relative contributions from the individual bands are shown, and the secondary jump at T_{TRSB} is highlighted with a red ring in (b).

IV. CONCLUSIONS

In this paper, we have examined the $d + ig$ -wave order parameter hypothesis as a candidate model for the superconductivity in SRO. We developed a generic multiband, multi-component Ginzburg–Landau theory for tetragonal lattice systems. We found that the theory favours comparable magnitudes of the d and g components at low temperature. On the other hand, the lack of observation of a second heat capacity jump¹⁶ requires the g -wave component to be less than about 30% of the d -wave component. Together, these two results place tight restrictions on any possible $d + ig$ scenario. Although the $d + ig$ candidate may reconcile a number of experiments, a robust justification for a near-degeneracy of d and g -wave order parameters is yet to be found. This outstanding issue is even more apparent when bearing in mind that numerous calculations based on realistic band structures have yet to find a competitive g -wave order parameter^{13,22–24,26,27,30,55–58}.

The continued squeezing of the range of acceptable theoretical scenarios compatible with experiment suggests that further experimental results might need revisiting. In the end, SRO might be more similar to the cuprates than previously thought, and interface experiments have hinted at time-reversal symmetry-invariant superconductivity⁵⁹. One could imagine the scenario of a cuprate-like $d_{x^2-y^2}$ -wave order parameter, where the apparent observation of TRSB originates from an anisotropic order parameter component caused by dislocations, magnetic de-

fects, or domain walls⁶⁰, or mechanisms not intrinsically related to superconductivity²⁹.

We also note that yet another order parameter candidate, of the form $d + ip$, has recently been suggested based on the near-degeneracy between even and odd-parity order parameters in the 1D Hubbard model⁶¹. This order can potentially reconcile junction experiments suggesting odd-parity order^{59,62–64} with other indications of a nodal d -wave^{10,11,13,14,20}. However, new NMR measurements²⁰ have made it clear that an odd-parity component must be subdominant ($\lesssim 10\%$ of the primary component).

The current experimental situation taken at face value appears to leave somewhat exotic options that at least would require further microscopic examination. These new hypotheses warrant careful (re-)examination in hopes of unifying theory and experiment to converge on a solution to the pairing symmetry puzzle in SRO.

ACKNOWLEDGMENTS

We thank Fabian Jerzembeck, Astrid Tranum Rømer, Catherine Kallin, Thomas Scaffidi, Steven Kivelson, and Alexander Balatsky for useful discussions. G. W. thanks the Kavli Institute for Theoretical Physics for its hospitality during the graduate fellowship programme. H. S. R. acknowledges support from the Aker Scholarship and VILLUM FONDEN via the Centre of Excellence for Dirac Materials (Grant No. 11744). F. F. acknowledges support from the Astor Junior Research Fellowship of New College, Oxford. S. H. S. is supported by EPSRC Grant No. EP/N01930X/1.

* henrik.roising@su.se

¹ Y. Maeno, H. Hashimoto, K. Yoshida, S. Nishizaki, T. Fujita, J. G. Bednorz, and F. Lichtenberg, *Nature* **372**, 532 (1994).
² A. P. Mackenzie and Y. Maeno, *Rev. Mod. Phys.* **75**, 657 (2003).
³ K. Ishida, H. Mukuda, Y. Kitaoka, K. Asayama, Z. Q. Mao, Y. Mori, and Y. Maeno, *Nature* **396**, 658–660 (1998).
⁴ G. M. Luke, Y. Fudamoto, K. M. Kojima, M. I. Larkin, J. Merrin, B. Nachumi, Y. J. Uemura, Y. Maeno, Z. Q. Mao, Y. Mori, H. Nakamura, and M. Sgrist, *Nature* **394**, 0028 (1998).
⁵ J. Xia, Y. Maeno, P. T. Beyersdorf, M. M. Fejer, and A. Kapitulnik, *Phys. Rev. Lett.* **97**, 167002 (2006).
⁶ C. Nayak, S. H. Simon, A. Stern, M. Freedman, and S. Das Sarma, *Rev. Mod. Phys.* **80**, 1083 (2008).
⁷ A. P. Mackenzie, T. Scaffidi, C. W. Hicks, and Y. Maeno, *npj Quantum Materials* **2** (2017).
⁸ S. NishiZaki, Y. Maeno, and Z. Mao, *J. Phys. Soc. Jpn.* **69**, 572 (2000).
⁹ M. J. Graf and A. V. Balatsky, *Phys. Rev. B* **62**, 9697 (2000).
¹⁰ E. Hassinger, P. Bourgeois-Hope, H. Taniguchi, S. René de Cotret, G. Grissonnanche, M. S. Anwar, Y. Maeno,

N. Doiron-Leyraud, and L. Taillefer, *Phys. Rev. X* **7**, 011032 (2017).
¹¹ R. Sharma, S. D. Edkins, Z. Wang, A. Kostin, C. Sow, Y. Maeno, A. P. Mackenzie, J. C. S. Davis, and V. Madhavan, *PNAS* **117**, 5222 (2020).
¹² C. W. Hicks, D. O. Brodsky, E. A. Yelland, A. S. Gibbs, J. A. N. Bruin, M. E. Barber, S. D. Edkins, K. Nishimura, S. Yonezawa, Y. Maeno, and A. P. Mackenzie, *Science* **344**, 283 (2014).
¹³ A. Steppke, L. Zhao, M. E. Barber, T. Scaffidi, F. Jerzembeck, H. Rosner, A. S. Gibbs, Y. Maeno, S. H. Simon, A. P. Mackenzie, and C. W. Hicks, *Science* **355**, eaaf9398 (2017).
¹⁴ A. Pustogow, Y. Luo, A. Chronister, Y.-S. Su, D. A. Sokolov, F. Jerzembeck, A. P. Mackenzie, C. W. Hicks, N. Kikugawa, S. Raghu, and S. E. Bauer, E. D. Brown, *Nature* **574**, 72 (2019).
¹⁵ K. Ishida, M. Manago, K. Kinjo, and Y. Maeno, *J. Phys. Soc. Jpn.* **89**, 034712 (2020).
¹⁶ Y.-S. Li, N. Kikugawa, D. Sokolov, F. Jerzembeck, A. Gibbs, Y. Maeno, C. Hicks, M. Nicklas, and A. Mackenzie, [arXiv:1906.07597 \[cond-mat.supr-con\]](https://arxiv.org/abs/1906.07597) (2019).
¹⁷ A. N. Petsch, M. Zhu, M. Enderle, Z. Q. Mao, Y. Maeno, and S. M. Hayden, <https://arxiv.org/abs/2002.02856>

- [[cond-mat.supr-con](#)] (2020).
- 18 V. Grinenko, S. Ghosh, R. Sarkar, J.-C. Orain, A. Nikitin, M. Elender, D. Das, Z. Guguchia, F. Brückner, M. E. Barber, J. Park, N. Kikugawa, D. A. Sokolov, J. S. Bobowski, T. Miyoshi, Y. Maeno, A. P. Mackenzie, H. Luetkens, C. W. Hicks, and H.-H. Klauss, [arXiv:2001.08152 \[cond-mat.supr-con\]](#) (2019).
 - 19 S. Ghosh, A. Shekhter, F. Jerzembeck, N. Kikugawa, D. A. Sokolov, M. Brando, A. P. Mackenzie, C. W. Hicks, and B. J. Ramshaw, *Nat. Phys.* (2020).
 - 20 A. Chronister, A. Pustogow, N. Kikugawa, D. A. Sokolov, F. Jerzembeck, C. W. Hicks, A. P. Mackenzie, E. D. Bauer, and S. E. Brown, [arXiv:2007.13730 \[cond-mat.supr-con\]](#) (2020).
 - 21 X. Cai, B. M. Zakrzewski, Y. A. Ying, H.-Y. Kee, M. Sigrist, J. E. Ortmann, W. Sun, Z. Mao, and Y. Liu, [arXiv:2010.15800 \[cond-mat.supr-con\]](#) (2020).
 - 22 O. Gingras, R. Nourafkan, A.-M. S. Tremblay, and M. Côté, *Phys. Rev. Lett.* **123**, 217005 (2019).
 - 23 A. T. Rømer, D. D. Scherer, I. M. Eremin, P. J. Hirschfeld, and B. M. Andersen, *Phys. Rev. Lett.* **123**, 247001 (2019).
 - 24 H. S. Røising, T. Scaffidi, F. Flicker, G. F. Lange, and S. H. Simon, *Phys. Rev. Research* **1**, 033108 (2019).
 - 25 A. W. Lindquist and H.-Y. Kee, *Phys. Rev. Research* **2**, 032055 (2020).
 - 26 H. G. Suh, H. Menke, P. M. R. Brydon, C. Timm, A. Ramires, and D. F. Agterberg, *Phys. Rev. Research* **2**, 032023 (2020).
 - 27 Z. Wang, X. Wang, and C. Kallin, *Phys. Rev. B* **101**, 064507 (2020).
 - 28 S. A. Kivelson, A. C. Yuan, B. J. Ramshaw, and R. Thomale, *npj Quantum Materials* **5**, 43 (2020).
 - 29 S. Mazumdar, *Phys. Rev. Research* **2**, 023382 (2020).
 - 30 A. T. Rømer, A. Kreisel, M. A. Müller, P. J. Hirschfeld, I. M. Eremin, and B. M. Andersen, *Phys. Rev. B* **102**, 054506 (2020).
 - 31 R. Willa, [arXiv:2005.04124 \[cond-mat.supr-con\]](#) (2020).
 - 32 A. J. Leggett and Y. Liu, [arXiv:2010.15220 \[cond-mat.supr-con\]](#) (2020).
 - 33 C. Bergemann, S. R. Julian, A. P. Mackenzie, S. NishiZaki, and Y. Maeno, *Phys. Rev. Lett.* **84**, 2662 (2000).
 - 34 C. N. Veenstra, Z.-H. Zhu, M. Raichle, B. M. Ludbrook, A. Nicolaou, B. Slomski, G. Landolt, S. Kittaka, Y. Maeno, J. H. Dil, I. S. Elfimov, M. W. Haverkort, and A. Damascelli, *Phys. Rev. Lett.* **112**, 127002 (2014).
 - 35 R. A. Fisher, S. Kim, B. F. Woodfield, N. E. Phillips, L. Taillefer, K. Hasselbach, J. Flouquet, A. L. Giorgi, and J. L. Smith, *Phys. Rev. Lett.* **62**, 1411 (1989).
 - 36 L. P. Gor'kov, *J. Exptl. Theoret. Phys. (U.S.S.R)* **36**, 1364 (1959).
 - 37 S. K. Ghosh, M. Smidman, T. Shang, J. F. Annett, A. Hillier, J. Quintanilla, and H. Yuan, [arXiv:2003.04357 \[cond-mat.supr-con\]](#) (2020).
 - 38 W.-C. Lee, S.-C. Zhang, and C. Wu, *Phys. Rev. Lett.* **102**, 217002 (2009).
 - 39 S. Ran, C. Eckberg, Q.-P. Ding, Y. Furukawa, T. Metz, S. R. Saha, I.-L. Liu, M. Zic, H. Kim, J. Paglione, and N. P. Butch, *Science* **365**, 684 (2019).
 - 40 L. Jiao, S. Howard, S. Ran, Z. Wang, J. O. Rodriguez, M. Sigrist, Z. Wang, N. P. Butch, and V. Madhavan, *Nature* **579**, 523 (2020).
 - 41 T. T. M. Palstra, A. A. Menovsky, J. v. d. Berg, A. J. Dirkmaat, P. H. Kes, G. J. Nieuwenhuys, and J. A. Mydosh, *Phys. Rev. Lett.* **55**, 2727 (1985).
 - 42 E. R. Schemm, R. E. Baumbach, P. H. Tobash, F. Ronning, E. D. Bauer, and A. Kapitulnik, *Phys. Rev. B* **91**, 140506 (2015).
 - 43 M. Silaev and E. Babaev, *Phys. Rev. B* **85**, 134514 (2012).
 - 44 N. V. Orlova, A. A. Shanenko, M. V. Milošević, F. M. Peeters, A. V. Vagov, and V. M. Axt, *Phys. Rev. B* **87**, 134510 (2013).
 - 45 H. Bruus and K. Flensberg, *Many-Body Quantum Theory in Condensed Matter Physics* (Oxford University Press, 2004).
 - 46 R. L. Frank and M. Lemm, *Annales Henri Poincaré* **17**, 2285 (2016).
 - 47 A. A. Abrikosov, L. P. Gor'kov, and I. E. Dzyaloshinskiĭ, *J. Exptl. Theoret. Phys. (U.S.S.R)* **36**, 900 (1959).
 - 48 M. V. Sadovskii, *Diagrammatics* (World Scientific, 2006).
 - 49 M. Sigrist and K. Ueda, *Rev. Mod. Phys.* **63**, 239 (1991).
 - 50 R. Balian and N. R. Werthamer, *Phys. Rev.* **131**, 1553 (1963).
 - 51 F. Šimkovic, X.-W. Liu, Y. Deng, and E. Kozik, *Phys. Rev. B* **94**, 085106 (2016).
 - 52 Private communication with Helge Rosner.
 - 53 B. Zinkl and M. Sigrist, [arXiv:2009.10089 \[cond-mat.supr-con\]](#) (2020).
 - 54 Which is $\Delta C/(\gamma_n T_c) \approx 0.74 \pm 0.02$ where $\gamma_n = C/T$ is evaluated in the normal state^s.
 - 55 T. Scaffidi, J. C. Romers, and S. H. Simon, *Phys. Rev. B* **89**, 220510 (2014).
 - 56 J. F. Dodaro, Z. Wang, and C. Kallin, *Phys. Rev. B* **98**, 214520 (2018).
 - 57 L.-D. Zhang, W. Huang, F. Yang, and H. Yao, *Phys. Rev. B* **97**, 060510 (2018).
 - 58 W.-S. Wang, C.-C. Zhang, F.-C. Zhang, and Q.-H. Wang, *Phys. Rev. Lett.* **122**, 027002 (2019).
 - 59 S. Kashiwaya, K. Saitoh, H. Kashiwaya, M. Koyanagi, M. Sato, K. Yada, Y. Tanaka, and Y. Maeno, *Phys. Rev. B* **100**, 094530 (2019).
 - 60 R. Willa, M. Hecker, R. M. Fernandes, and J. Schmalian, [arXiv:2011.01941 \[cond-mat.supr-con\]](#) (2020).
 - 61 T. Scaffidi, [arXiv:2007.13769 \[cond-mat.supr-con\]](#) (2020).
 - 62 K. D. Nelson, Z. Q. Mao, Y. Maeno, and Y. Liu, *Science* **306**, 1151 (2004).
 - 63 F. Kidwingira, J. D. Strand, D. J. Van Harlingen, and Y. Maeno, *Science* **314**, 1267 (2006).
 - 64 M. S. Anwar, R. Ishiguro, T. Nakamura, M. Yakabe, S. Yonezawa, H. Takayanagi, and Y. Maeno, *Phys. Rev. B* **95**, 224509 (2017).
 - 65 M.-P. Chen and H. M. Srivastava, *Results in Mathematics* **33**, 179 (1998).
 - 66 M. Sigrist, *AIP Conf. Proc.* **789**, 165 (2005).

Appendix A: GL theory with full momentum dependence

The full momentum-dependent GL coefficients analogous to the momentum-independent expressions (10) and (11) from the main text are

$$\alpha_\mu(\mathbf{q}, T, T_c) = -V \int \frac{d\mathbf{p}}{(2\pi)^d} \frac{\tanh\left(\frac{\xi_\mu(\mathbf{p} + \frac{\mathbf{q}}{2})}{2T}\right) + \tanh\left(\frac{\xi_\mu(\mathbf{p} - \frac{\mathbf{q}}{2})}{2T}\right) - \tanh\left(\frac{\xi_\mu(\mathbf{p} + \frac{\mathbf{q}}{2})}{2T_c}\right) - \tanh\left(\frac{\xi_\mu(\mathbf{p} - \frac{\mathbf{q}}{2})}{2T_c}\right)}{2[\xi_\mu(\mathbf{p} + \frac{\mathbf{q}}{2}) + \xi_\mu(\mathbf{p} - \frac{\mathbf{q}}{2})]} \quad (\text{A1})$$

and

$$\begin{aligned} \beta_\mu(\mathbf{q}_1, \mathbf{q}_2, \mathbf{q}_3, T) = V \int \frac{d\mathbf{p}}{(2\pi)^d} & \times \left\{ \frac{\tanh\left(\frac{\xi_\mu(\mathbf{p})}{2T}\right)}{2[\xi_\mu(\mathbf{p}) + \xi_\mu(\mathbf{p} + \mathbf{q}_1)][\xi_\mu(\mathbf{p} + \mathbf{q}_1 - \mathbf{q}_3) - \xi_\mu(\mathbf{p})][\xi_\mu(\mathbf{p}) + \xi_\mu(\mathbf{p} + \mathbf{q}_1 + \mathbf{q}_2 - \mathbf{q}_3)]} \right. \\ & - \frac{\tanh\left(\frac{\xi_\mu(\mathbf{p} + \mathbf{q}_1)}{2T}\right)}{2[\xi_\mu(\mathbf{p}) + \xi_\mu(\mathbf{p} + \mathbf{q}_1)][\xi_\mu(\mathbf{p} + \mathbf{q}_1 - \mathbf{q}_3) + \xi_\mu(\mathbf{p} + \mathbf{q}_1)][\xi_\mu(\mathbf{p} + \mathbf{q}_1) - \xi_\mu(\mathbf{p} + \mathbf{q}_1 + \mathbf{q}_2 - \mathbf{q}_3)]} \\ & - \frac{\tanh\left(\frac{\xi_\mu(\mathbf{p} + \mathbf{q}_1 - \mathbf{q}_3)}{2T}\right)}{2[\xi_\mu(\mathbf{p} + \mathbf{q}_1 - \mathbf{q}_3) - \xi_\mu(\mathbf{p})][\xi_\mu(\mathbf{p} + \mathbf{q}_1 - \mathbf{q}_3) + \xi_\mu(\mathbf{p} + \mathbf{q}_1)][\xi_\mu(\mathbf{p} + \mathbf{q}_1 - \mathbf{q}_3) + \xi_\mu(\mathbf{p} + \mathbf{q}_1 + \mathbf{q}_2 - \mathbf{q}_3)]} \\ & \left. + \frac{\tanh\left(\frac{\xi_\mu(\mathbf{p} + \mathbf{q}_1 + \mathbf{q}_2 - \mathbf{q}_3)}{2T}\right)}{2[\xi_\mu(\mathbf{p} + \mathbf{q}_1 - \mathbf{q}_3) + \xi_\mu(\mathbf{p} + \mathbf{q}_1 + \mathbf{q}_2 - \mathbf{q}_3)][\xi_\mu(\mathbf{p} + \mathbf{q}_1) - \xi_\mu(\mathbf{p} + \mathbf{q}_1 + \mathbf{q}_2 - \mathbf{q}_3)][\xi_\mu(\mathbf{p}) + \xi_\mu(\mathbf{p} + \mathbf{q}_1 + \mathbf{q}_2 - \mathbf{q}_3)]} \right\}. \quad (\text{A2}) \end{aligned}$$

The free energy is then

$$\begin{aligned} F_2[\{\Delta_{a\mu}, \Delta_{b\mu}\}] = \sum_\mu \left(\sum_{\mathbf{q}} \alpha_\mu(\mathbf{q}, T, T_c) |\Delta_{a\mu}(\mathbf{q})|^2 + \alpha_\mu(\mathbf{q}, T, T_c) |\Delta_{b\mu}(\mathbf{q})|^2 \right. \\ \left. + \sum_{\mathbf{q}_1, \mathbf{q}_2, \mathbf{q}_3} \beta_\mu(\mathbf{q}_1, \mathbf{q}_2, \mathbf{q}_3, T_c) \sum_{ijkl} f_{ijkl} \Delta_{i\mu}^*(\mathbf{q}_1) \Delta_{j\mu}^*(\mathbf{q}_2) \Delta_{k\mu}(\mathbf{q}_3) \Delta_{l\mu}(\mathbf{q}_1 + \mathbf{q}_2 - \mathbf{q}_3) \right) \quad (\text{A3}) \end{aligned}$$

If we write the gap functions as $\Delta_{a\mu}(\mathbf{q}) = \Delta_0 \tilde{\Delta}_{a\mu}(\mathbf{q})$ and $\Delta_{b\mu}(\mathbf{q}) = iX \Delta_0 \tilde{\Delta}_{b\mu}(\mathbf{q})$ where $\tilde{\Delta}_{a/b\mu}(\mathbf{q})$ are the normalized gap functions and X is assumed to be real, then we will have a free energy of the form

$$F_2[\Delta_0, X] = \Delta_0^2(a + bX^2) + \Delta_0^4(c + dX^2 + eX^4), \quad (\text{A4})$$

where a, b, c, d, e are coefficients determined from the Monte-Carlo integration. For thermodynamic stability we will require $c, e > 0$ and $d^2 < 4ec$ if $d < 0$. We need to handle the integrand

$$\beta_{\text{int}}(x, y, w, z) = \frac{\tanh \frac{x}{2}}{2(x+y)(w-x)(x+z)} - \frac{\tanh \frac{y}{2}}{2(x+y)(w+y)(y-z)} - \frac{\tanh \frac{w}{2}}{2(w-x)(w+y)(w+z)} + \frac{\tanh \frac{z}{2}}{2(w+z)(y-z)(x+z)}, \quad (\text{A5})$$

where $x = \xi_\mu(\mathbf{p})$, $y = \xi_\mu(\mathbf{p} + \mathbf{q}_1)$, $w = \xi_\mu(\mathbf{p} + \mathbf{q}_1 - \mathbf{q}_3)$, $z = \xi_\mu(\mathbf{p} + \mathbf{q}_1 + \mathbf{q}_2 - \mathbf{q}_3)$. This integrand needs to be treated carefully since it has a number of points where both numerator and denominator vanish, such as when $x = -y$. Close to these special points, we need to switch to alternative expressions which are regular about these points. In particular, if two arguments collide

$$\beta_{\text{int}}(x, -x, w, z) = \frac{-2(w-x)^2 \tanh\left(\frac{z}{2}\right) - 2 \tanh\left(\frac{w}{2}\right) (x+z)^2 + (w+z) \text{sech}^2\left(\frac{x}{2}\right) ((w-x)(x+z) + \sinh(x)(-w+2x+z))}{4(w-x)^2(w+z)(x+z)^2}, \quad (\text{A6})$$

and if three arguments collide

$$\beta_{\text{int}}(x, -x, x, z) = \frac{\text{sech}^2\left(\frac{x}{2}\right) ((x+z) ((x+z) \tanh\left(\frac{x}{2}\right) + 2) - 2 \sinh(x)) - 4 \tanh\left(\frac{z}{2}\right)}{8(x+z)^3}, \quad (\text{A7})$$

and for all four arguments colliding

$$\beta_{\text{int}}(x, -x, x, -x) = -\frac{1}{48}(\cosh(x) - 2)\text{sech}^4\left(\frac{x}{2}\right). \quad (\text{A8})$$

Minimizing the free energy (A4) with respect to Δ_0 and X leads to

$$X^2 = \frac{ad - 2bc}{bd - 2ea}, \quad (\text{A9})$$

such that $X^2 < 0$ for $T > T_{\text{TRSB}}$. Using the approximate temperature dependence $a = -a_0(1 - T/T_c)$ and $b = -b_0(1 - T/T'_c)$ we find

$$X(T) = \sqrt{\frac{(a_0d - 2b_0c)(1 - \frac{T}{T_{\text{TRSB}}})}{b_0d(1 - \frac{T}{T'_c}) - 2ea_0(1 - \frac{T}{T_c)}}} \quad (\text{A10})$$

for $T < T_{\text{TRSB}}$, where

$$T_{\text{TRSB}} = T'_c \frac{1 - \frac{a_0d}{2b_0c}}{1 - \frac{a_0d}{2b_0c} \frac{T'_c}{T_c}}. \quad (\text{A11})$$

Appendix B: Series representations for Apéry's constant

To evaluate the basic integral of Eq. (11) in the low-filling 2D limit, $\frac{1}{2} \int_0^\infty du \frac{\sinh u - u}{4u^3(1 + \cosh u)}$, one can make use of the following series expansions:

$$\frac{2}{1 + \cosh(x)} = \cosh^{-2}(x/2) = 4e^{-x} \sum_{n=0}^{\infty} (-1)^n (1+n)e^{-nx}, \quad (\text{B1})$$

$$\sinh(x) - x = \frac{\sqrt{\pi}}{2} \sum_{m=1}^{\infty} \frac{x^{2m+1}}{4^m \Gamma(m+1) \Gamma(m + \frac{3}{2})}, \quad (\text{B2})$$

$$\sum_{n=0}^{\infty} (-1)^n \frac{1}{(1+n)^x} = (1 - 2^{1-x}) \zeta(x). \quad (\text{B3})$$

By equating the resulting expression for β_μ with the result derived by Gor'kov³⁶, we find that

$$\begin{aligned} \frac{7\zeta(3)}{32\pi^2} &= \frac{\sqrt{\pi}}{8} \sum_{l=1}^{\infty} (1 - 2^{3-2l}) \frac{\Gamma(2l-1)}{4^l \Gamma(l+1) \Gamma(l + \frac{3}{2})} \zeta(2l-2) \Rightarrow \\ \zeta(3) &= \frac{8\pi^2}{7} \sum_{n=0}^{\infty} \frac{(1 - 2 \cdot 2^{-2n}) \zeta(2n)}{(2n+1)(2n+2)(2n+3)}, \end{aligned} \quad (\text{B4})$$

where $\zeta(0) = -1/2$. In fact, both of the terms inside the sum of Eq. (B4) individually yield a series expansion for $\zeta(3)$:

$$\zeta(3) = -\frac{8\pi^2}{5} \sum_{n=0}^{\infty} \frac{\zeta(2n)}{(2n+1)(2n+2)(2n+3)2^{2n}}, \quad (\text{B5})$$

$$\zeta(3) = -\frac{8\pi^2}{3} \sum_{n=0}^{\infty} \frac{\zeta(2n)}{(2n+1)(2n+2)(2n+3)}. \quad (\text{B6})$$

The most rapidly convergent series of the two, Eq. (B5), along with plenty of other variations, was discovered by Chen and Srivastava⁶⁵. The latter one, however, does not appear to have been discussed in the literature.

TABLE II. Tight-binding parameters for Eqs. (C2) and (C3).

Parameter	t_1	t_2	t_3	t_4	t_5	t_6	μ_{1D}	λ
Value [meV]	296.2	-57.3	52.6	-15.6	-15.1	-11.6	315.6	-50.7

TABLE III. Tight-binding parameters for Eq. (C4).

Parameter	\bar{t}_1	\bar{t}_2	\bar{t}_3	\bar{t}_4	\bar{t}_5	\bar{t}_6	\bar{t}_7	μ_{2D}
Value [meV]	369.5	123.2	20.4	13.9	-6.0	3.2	2.8	432.5

Appendix C: Tight-binding model

We consider an effective yet accurate two-dimensional, three-band, tight-binding model for Sr_2RuO_4 based on density functional theory (DFT)^{13,52},

$$H_K = \sum_{\mathbf{k}, s} \psi_s^\dagger(\mathbf{k}) h_s(\mathbf{k}) \psi_s(\mathbf{k}), \quad (\text{C1})$$

where $\psi_s(\mathbf{k}) = [c_{xz,s}(\mathbf{k}), c_{yz,s}(\mathbf{k}), c_{xy,-s}(\mathbf{k})]^T$ and where $s \in \{\uparrow, \downarrow\}$ denotes spin. The matrix $h_s(\mathbf{k})$ is well approximated by the 3×3 block diagonal matrix

$$h_s(\mathbf{k}) = \begin{pmatrix} \varepsilon_{xz}(\mathbf{k}) & -is\lambda & i\lambda \\ is\lambda & \varepsilon_{yz}(\mathbf{k}) & -s\lambda \\ -i\lambda & -s\lambda & \varepsilon_{xy}(\mathbf{k}) \end{pmatrix}, \quad (\text{C2})$$

where spin-orbit coupling is parametrized by λ , and the above energies are given by

$$\begin{aligned} \varepsilon_{1D}(k_{\parallel}, k_{\perp}) &= -2t_1 \cos k_{\parallel} - 2t_2 \cos(2k_{\parallel}) - 2t_3 \cos k_{\perp} - 4t_4 \cos k_{\parallel} \cos k_{\perp} \\ &\quad - 4t_5 \cos(2k_{\parallel}) \cos k_{\perp} - 2t_6 \cos(3k_{\parallel}) - \mu_{1D}, \end{aligned} \quad (\text{C3})$$

$$\begin{aligned} \varepsilon_{2D}(k_x, k_y) &= -2\bar{t}_1 [\cos k_x + \cos k_y] - 4\bar{t}_2 \cos k_x \cos k_y \\ &\quad - 4\bar{t}_3 [\cos(2k_x) \cos(k_y) + \cos(2k_y) \cos(k_x)] - 4\bar{t}_4 \cos(2k_x) \cos(2k_y) \\ &\quad - 2\bar{t}_5 [\cos(2k_x) + \cos(2k_y)] - 4\bar{t}_6 [\cos(3k_x) \cos(k_y) + \cos(3k_y) \cos(k_x)] \\ &\quad - 4\bar{t}_7 [\cos(3k_x) + \cos(3k_y)] - \mu_{2D}, \end{aligned} \quad (\text{C4})$$

with the identifications $\varepsilon_{xz}(\mathbf{k}) = \varepsilon_{1D}(k_x, k_y)$, $\varepsilon_{yz}(\mathbf{k}) = \varepsilon_{1D}(k_y, k_x)$, and $\varepsilon_{xy}(\mathbf{k}) = \varepsilon_{2D}(k_x, k_y)$. The tight-binding parameters consistent with DFT data are given in Table II and III. Serving as a benchmark calculation the relative band densities at the Fermi level produced with this model are $\rho_{\mu}/\rho_{\text{tot}} = 0.163, 0.314, 0.523$ for $\mu = \alpha, \beta, \gamma$, respectively, with

$$\rho_{\mu} = \int_{S_{\mu}} \frac{d\mathbf{k}}{(2\pi)^2} \frac{1}{|\nabla \xi_{\mu}(\mathbf{k})|}, \quad (\text{C5})$$

where S_{μ} is the Fermi surface sheet corresponding to band μ .

Appendix D: Order parameters and further plots

The lattice harmonics for the order parameters of Tab. I are in general band-dependent. It turns out that the microscopically obtained gap structures of Ref. 24 (at $J/U = 0.20$) can be well described by the lowest three lattice harmonics. The result of a fitting procedure of the order parameters of symmetries A_{1g} , A_{2g} , B_{1g} , and B_{2g} are shown in Table IV and V.

To supplement the results for the heat capacity ratio η shown in Fig. 5, Fig. 6 shows the result of the same calculation using only the leading lattice harmonic. Comparing the two figures demonstrates that the results are

TABLE IV. Lattice harmonics coefficients of the A_{1g} and A_{2g} order parameter (see Tab. I) obtained at $J/U = 0.20$ of Ref. 24, normalized such that $\max_{\theta,\mu} \Delta_{\alpha\mu}(\theta) = 1$.

μ	$a_{1,\mu}$	$a_{2,\mu}$	$a_{3,\mu}$	μ	$b_{0,\mu}$	$b_{1,\mu}$	$b_{2,\mu}$
α	+0.855	+0.007	+0.067	α	+0.269	-0.127	+0.038
β	-0.225	-0.329	+0.116	β	-0.895	-0.062	+0.052
γ	-0.097	-0.296	-0.303	γ	-0.022	-0.219	+0.150

TABLE V. Same as in Table IV but for symmetry channels B_{1g} and B_{2g} (see Tab. I).

μ	$c_{0,\mu}$	$c_{1,\mu}$	$c_{2,\mu}$	μ	$d_{0,\mu}$	$d_{1,\mu}$	$d_{2,\mu}$
α	-0.912	-0.011	-0.078	α	-0.120	+0.010	-0.051
β	+0.783	+0.143	+0.022	β	+0.943	-0.060	-0.099
γ	+0.358	+0.288	-0.007	γ	-0.492	-0.230	+0.0004

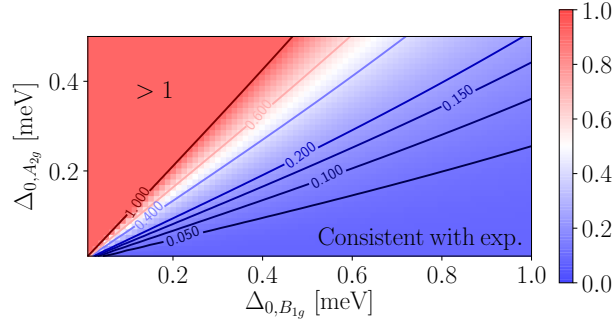


FIG. 6. The same as described in the caption of Fig. 5 but using only the leading lattice harmonics from Table I for the order parameters.

fairly insensitive to the precise structure of the gap. Moreover, Fig. 7 shows the outcome of the same calculation for the alternative order parameter combination $A_{1g} + iB_{2g}$, using the three leading lattice harmonics from Table IV and V here, respectively. Finally, Fig. 8 shows the results of minimizing the GL theory of Sec. II C for the $A_{1g} + iB_{2g}$

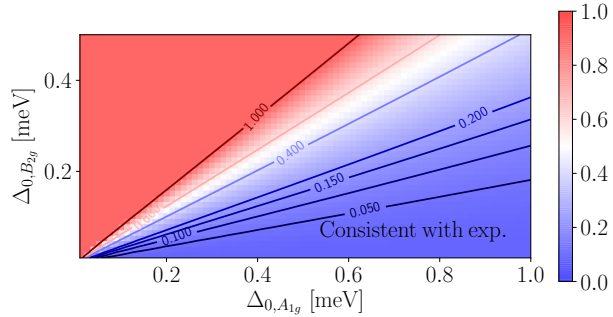


FIG. 7. The same as described in the caption of Fig. 5 but here for an order parameter of the form $A_{1g} + iB_{2g}$, using the advanced order parameters with the three leading lattice harmonics from Table IV and V.

order parameter.

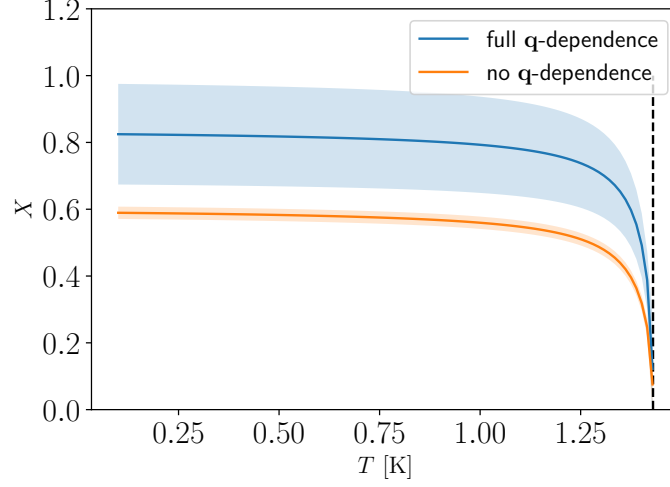


FIG. 8. The weight $X(T)$, with an order parameter of the form $\Delta(\mathbf{k}) = \Delta_0(T)[\Delta_{A_{1g}\mu}(\mathbf{k}) + iX(T)\Delta_{B_{2g}\mu}(\mathbf{k})]$ for $T_{\text{TRSB}} = 1.43$ K (indicated by the dashed line) and $T_c = 1.48$ K. The approximate result is obtained from the momentum-independent GL coefficients Eqs. (10) and (11), whereas the exact result is obtained from the full momentum-dependent expressions Eqs. (8) and (9).

Appendix E: Sign of the second heat capacity jump

The heat capacity jump at T_{TRSB} is determined by the discontinuity in $\partial|\Delta|^2/\partial T$, as seen from the normalized expression (the constant γ_n below is defined such that $1 = C(T)/(T\gamma_n)|_{T>T_c}$)⁶⁶

$$\frac{C(T)}{T\gamma_n} = \frac{3}{4\pi^2(k_B T)^3 \sum_\nu \rho_\nu} \int_{-\infty}^{\infty} d\xi \left\langle \frac{\xi^2 + |\Delta_\mu(\mathbf{k}, T)|^2 - \frac{T}{2} \frac{\partial |\Delta_\mu(\mathbf{k}, T)|^2}{\partial T}}{\cosh^2\left(\frac{E_\mu(\mathbf{k})}{2k_B T}\right)} \right\rangle_{\text{FS}}, \quad (\text{E1})$$

where the Fermi surface average is evaluated as

$$\langle A \rangle_{\text{FS}} \equiv \sum_\mu \frac{\rho_\mu}{|S_\mu|} \int_{S_\mu} d\mathbf{k} A. \quad (\text{E2})$$

Here ρ_μ is the density of states on band μ (see Appendix C), and $|S_\mu|$ is the area of the corresponding Fermi surface sheet. Assuming a gap function

$$\Delta_\mu(\mathbf{k}, T) = \Delta_0(T)[\Delta_{m\mu}(\mathbf{k}) + iX(T)\Delta_{n\mu}(\mathbf{k})], \quad (\text{E3})$$

with m and n being symmetry labels, and using the results from minimizing the free energy of Eq. (A4)

$$X(T)^2 = \begin{cases} \frac{ad-2bc}{bd-2ea} & \text{for } T < T_{\text{TRSB}} \\ 0 & \text{for } T > T_{\text{TRSB}}, \end{cases} \quad (\text{E4})$$

and

$$\Delta_0(T)^2 = \begin{cases} -\frac{bd-2ea}{d^2-4ec} & \text{for } T < T_{\text{TRSB}} \\ -\frac{a}{2c} & \text{for } T_{\text{TRSB}} < T < T_c \\ 0 & \text{for } T > T_c, \end{cases} \quad (\text{E5})$$

one can derive

$$\frac{\partial |\Delta_\mu(\mathbf{k}, T)|^2}{\partial T} \Big|_{T_{\text{TRSB}}-\varepsilon}^{T_{\text{TRSB}}+\varepsilon} = \frac{a_0}{T_c} d - 2\frac{b_0}{T_c} c \left(-\frac{d}{2c} \Delta_{m\mu}(\mathbf{k})^2 + \Delta_{n\mu}(\mathbf{k})^2 \right). \quad (\text{E6})$$

For $d < 0$, the thermodynamic stability condition implies that this quantity is always positive definite, resulting in a positive heat capacity jump. However, for $d > 0$, the sign of the expression in Eq. (E6) is undetermined and in particular when averaged over the Fermi surface it can have either sign, resulting in either a positive or negative heat capacity jump. Cancellations between bands can result in a smaller second heat capacity jump.